Superhydrophobic ZnO/TiO$_2$ heterostructure with significantly enhanced photocatalytic activity

Diliraj Upadhaya[1] · **Pankaj Kumar**[1] · **Debarun Dhar Purkayastha**[1]

Abstract

ZnO/TiO$_2$ and TiO$_2$/ZnO thin films were prepared on borosilicate glass slide (BSG) by cost effective sol–gel spin coating technique. The films were characterized using X-ray diffraction, FESEM and FT-IR. The X-ray diffraction reveals the existence of both hexagonal ZnO and anatase TiO$_2$ phases for ZnO/TiO$_2$ and TiO$_2$/ZnO thin films. In the present work, an effort has been made to systematically study the wettability and photocatalytic activity of ZnO/TiO$_2$ and TiO$_2$/ZnO thin films. The wettability of the films was assessed by measuring the water contact angle (WCA). The WCA of ZnO/TiO$_2$ and TiO$_2$/ZnO was 43.6º and 26.3º respectively. The WCA of the films increases by modifying with octadecanoic acid (OA) where ZnO/TiO$_2$ shows superhydrophobic nature having WCA of 151.0º. The photocatalytic activities of the films were evaluated by measuring the degradation of methylene blue (MB) and octadecanoic acid under UV light. The photocatalytic efficiency of ZnO/TiO$_2$ was higher because of the formation of heterostructure which inhibits the charge recombination.

1 Introduction

Environmental contamination has become a pressing dilemma to all forms of biodiversity on earth. The expulsion of harmful organic complexes from various industries into water bodies has further added perplexity to the situation [1]. The disintegration of organic complexes by the photocatalytic degradation process (PDP) has been a focus of numerous research establishments [2–4]. In this light, the role of semiconductor photocatalyst (TiO$_2$, ZnO, SnO$_2$ etc.) for PDP has been extensively studied. The motive of choosing semiconductors photocatalyst for PDP is due to their non-toxicity, chemical inertness, photostablility, cost-effective and their ability to utilize visible and/or UV light [5, 6]. In a symbolic process when a semiconductor photocatalyst is irradiated with photons of energy equal or higher than the band gap energy, the electrons from the valence band will move to the conduction band leaving a hole in the valence band. The electrons and hole pairs so generated undergoes redox reaction with organic compound adsorbed on the surface and disintegrate them. The main drawback of single phase semiconductor photocatalyst is the quick reunion of photogenerated electron–hole pairs and narrow light-response region. There are reports of enhancing the photocatalytic efficiency by doping with metals [7]. However, the formation of heterostructures by using two or more semiconductors has shown a promising sign in enriching the photocatalytic performance [8–10]. The formation of heterostructures extends the photoactive region and electron–hole pair efficiency. Hence a large number of semiconductor heterostructures such as SnO$_2$–TiO$_2$, TiO$_2$–CdS, ZnO–SnO$_2$, TiO$_2$–Fe$_2$O$_3$ etc. were studied and used for photocatalytic applications [11–14]. Among various metal oxide semiconductors, TiO$_2$ (3.2 eV) and ZnO (3.37 eV) are noted direct band gap semiconductor with comparable band gap. They are found to have promising applications in self cleaning, photocatalysis and so on [15].

In the present work, a heterostructure of ZnO/TiO$_2$ and TiO$_2$/ZnO was deposited on borosilicate glass (BSG) substrate by cost-effective spin coating technique. There are various methods of deposition of thin films such as thermal evaporation, sputtering, sol–gel etc. [16–18]. Sol–gel spin coating process stands out to be better among various thin film deposition techniques due to its simplicity in processing, low temperature process, superior control on

✉ Debarun Dhar Purkayastha
  ddebarun@yahoo.com

1 Department of Physics, National Institute of Technology Nagaland, Chumukedima, Dimapur 797103, India

the composition and homogeneity [19]. In the past many groups have reported about the photocatalytic degradation of organic complexes by using ZnO/TiO_2 as photocatalyst [20–23]. However, to the best of present author's knowledge, there are no studies concerning the wetting behavior of ZnO/TiO_2 and TiO_2/ZnO heterostructures and its photo degradation of organic pollutants in solid phase (octadecanoic acid) and liquid phase (methylene blue).

2 Experimental

Nanostructured thin films of ZnO/TiO_2 (ZnO at the top and TiO_2 at the bottom) and TiO_2/ZnO (TiO_2 at the top and ZnO at the bottom) was prepared on borosilicate glass substrate (BSG) by cost effective sol–gel spin coating technique. TiO_2 sol was prepared by using titanium isopropoxide as the precursor [24]. At first, isopropanol was added drop by drop into the precursor solution. The solution was stirred under heating at 60° C for 10 min. To this, acetic acid was poured under continuous stirring for 15 min at 60° C followed by addition of methanol and stirred for 2 h at 60 °C. Alternatively, ZnO sol was prepared by using zinc acetate dehydrate (ZAD) as precursor [25]. At first, ZAD was dissolved in 2-methoxyethanol and stirred at 60 °C for 30 min. This was followed by addition of monoethanol amine (MEA) under stirring at 60 °C for another 2 h resulting in the formation of a clear and homogeneous sol. The sol was kept to age for 24 h at 50° C. The molar ratio of MEA to ZAD was fixed at 1:1. Prior to the deposition, glass substrates were cleaned with ethanol, sonicated in acetone and then dried at 100 °C for 30 min to remove impurities. In order to make a uniform layer, the spin parameters for coating the sol were kept at 500 rpm for 10 s and 3000 rpm for the next 30 s for all the films. TiO_2 films were deposited from the prepared sol and dried at 120° C after each coating and then annealed at 500° C for 2 h. Then ZnO sol was coated over TiO_2, dried at 120 °C and subsequently annealed at 500 °C to get ZnO/TiO_2 films. Similarly, TiO_2/ZnO films were prepared by coating TiO_2 over ZnO by maintaining the same experimental conditions like that of ZnO/TiO_2 films. The formation of bilayer structure could lead to band gap engineering by forming heterostructures which enhances the photocatalytic properties [26]. The thickness of all the films were kept constant by depositing equal number of layers for TiO_2, ZnO, ZnO/TiO_2 and TiO_2/ZnO thin films.

The crystallinity of the films were evaluated by grazing incident X-ray diffraction (Rigaku Ultima IV) using Cu Kα radiation of wavelength 0.15405 nm in the 2θ range of 20°–80°. A UV–Vis Spectrophotometer (Agilent Cary 60) over the wavelength range 200–800 nm was used to record the absorbance of dye after UV irradiation. The Fourier Transform Infra-red (FTIR) spectra (Agilent Cary 630)

were recorded with 4000–450 cm^{-1} as the spectral range. Contact Angle goniometer (DMs-401, Kyowa Interface Science CO Limited, Japan) was used for contact angle studies by sessile drop mode. The surface energies of the samples were determined by Owens–Wendt geometric mean method using a polar (deionized water) and a non-polar liquid (diiodomethane). The volume of each liquid was 2 μl for contact angle measurement. The elemental contents and surface morphology were obtained by Field emission scanning electron microscope (FEG-SEM, JSM-7600F) connected with Energy Dispersive X-ray (EDX) analyzer. The photocatalytic performances of the films were evaluated by measuring the degradation of methylene blue (MB) and octadecanoic acid (OA) with UV-irradiation. The UV lamp (6 W) was used as irradiation source for determination of photocatalytic activity ($\lambda = 254$ nm). The demineralization of the dye was investigated by performing total organic carbon (TOC) analysis by using TOC analyser O.I analytical solid (Model no-1030 with auto sampler).

3 Results and discussion

The X-ray diffraction patterns of ZnO, TiO_2, TiO_2/ZnO and ZnO/TiO_2 thin films are presented in Fig. 1. The diffraction peaks in XRD confirms the hexagonal wurtzite structure of ZnO (JCPDS No. 89-1397) for ZnO films and anatase TiO_2 (JCPDS No. 89-4921) for TiO_2 films. The existence of ZnO hexagonal and TiO_2 anatase phase are evident in both TiO_2/ZnO and ZnO/TiO_2 thin films respectively. The films show sharp diffraction peaks indicating the high crystallinity of both ZnO and TiO_2. No extra peaks other than hexagonal
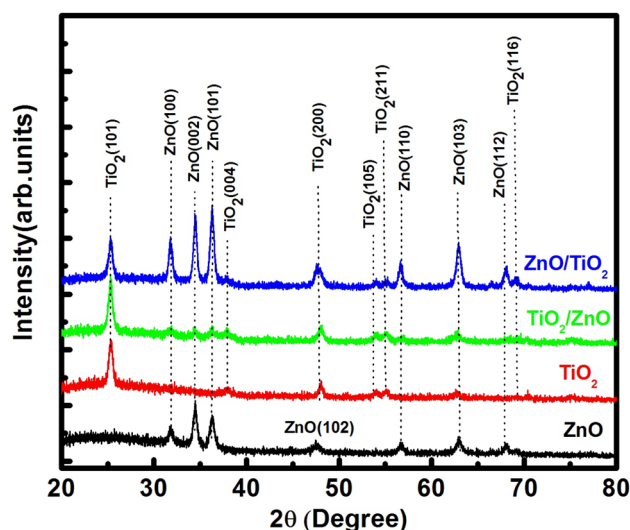

Fig. 1 X-ray diffraction patterns of TiO_2, ZnO, TiO_2/ZnO and ZnO/TiO_2 thin films

wurtzite of ZnO and anatase of TiO_2 were observed. Further the average crystallites size (taking all peaks) was estimated by Scherrer's formula [17].

$$D = \frac{0.9\lambda}{\beta \cos\theta} \qquad (1)$$

where $\lambda = 0.15405$ nm is the wavelength of incident Cu Kα radiation, β is the full width half maxima and θ is the angle due to Bragg's diffraction.

The crystallite size of TiO_2 and ZnO was measured to be 21.2 nm and 17.9 nm respectively. In case of TiO_2/ZnO, the crystallite size of TiO_2 was found to be 18.2 nm where as the crystallite size for ZnO was found to be 18.5 nm. On the other hand, the crystallite size of TiO_2 and ZnO was found to be 16 nm and 20.5 nm respectively for ZnO/TiO_2. Hence it can be seen that the presence of TiO_2 increases the crystallite size of ZnO where as ZnO restrains the growth of TiO_2 nano crystals in TiO_2/ZnO and ZnO/TiO_2.

The FESEM micrographs of TiO_2, ZnO, TiO_2/ZnO and ZnO/TiO_2 are shown in Fig. 2. The FESEM images show granular structure for TiO_2, ZnO and TiO_2/ZnO. The particle size of TiO_2, ZnO and TiO_2/ZnO thin films was found to be 23 nm, 18 nm and 20 nm respectively. In case of ZnO/TiO_2, non uniform agglomeration of nanoparticles with branch type clusters of various sizes are observed. The EDX spectra of TiO_2, ZnO, TiO_2/ZnO and ZnO/TiO_2 thin films are depicted in Fig. 3. EDX analysis indicates the existence of Ti and O in TiO_2, Zn and O in ZnO and Ti, Zn and O in TiO_2/ZnO and ZnO/TiO_2 thin films respectively. The peaks of silicon, sodium and calcium are due to borosilicate glass.

Moreover, footprints of carbon and gold are seen, which are due to carbon tape used for pasting the sample in the stub and gold coating on the films respectively. The thickness of ZnO/TiO_2 film calculated from cross-sectional FESEM image (available in Figure S1 in supporting file). The thickness of ZnO/TiO_2 is found to be 150 nm approximately.

The surface wettability involves the interaction of liquid with the solid interface. Young proposed a theoretical equation relating liquid contact angle on a solid surface [27]. The contact angle is related to surface energy where low surface energy leads to higher contact angle and vice versa. The component of surface energy of the films was calculated by Owens–Wendt geometric mean method [28].

$$(1 + \cos\theta)\sigma_{LV} = 2\sqrt{\sigma_S^P \sigma_L^P} + 2\sqrt{\sigma_S^D \sigma_L^D} \qquad (2)$$

where $\sigma_L^P, \sigma_L^D, \sigma_S^P, \sigma_S^D$ represent polar and dispersive components of the surface energy of liquid and solid respectively.

The drop profile, water contact angle (WCA) and surface energy of as deposited and octadecanoic acid modified TiO_2, ZnO, TiO_2/ZnO and ZnO/TiO_2 thin films are depicted in Table 1. The WCA of as deposited TiO_2 film is 16.9º and total surface energy is 70.7 mJ/m^2 ($\sigma_S^D = 29.2$ mJ/m^2, $\sigma_S^P = 41.5$ mJ/m^2). The as deposited ZnO films has WCA of 75.3º and total surface energy as 35.2 mJ/m^2 ($\sigma_S^D = 25.7$ mJ/m^2, $\sigma_S^P = 9.5$ mJ/m^2) where as the WCA and total surface energy of as deposited TiO_2/ZnO and ZnO/TiO_2 films are 26.3º, 67.2 mJ/m^2 ($\sigma_S^D = 30.8$ mJ/m^2, $\sigma_S^P = 36.4$ mJ/m^2) and 43.6º, 56.8 mJ/m^2 ($\sigma_S^D = 29.3$ mJ/m^2, $\sigma_S^P = 27.5$ mJ/m^2) respectively. The low surface energy in case of ZnO/

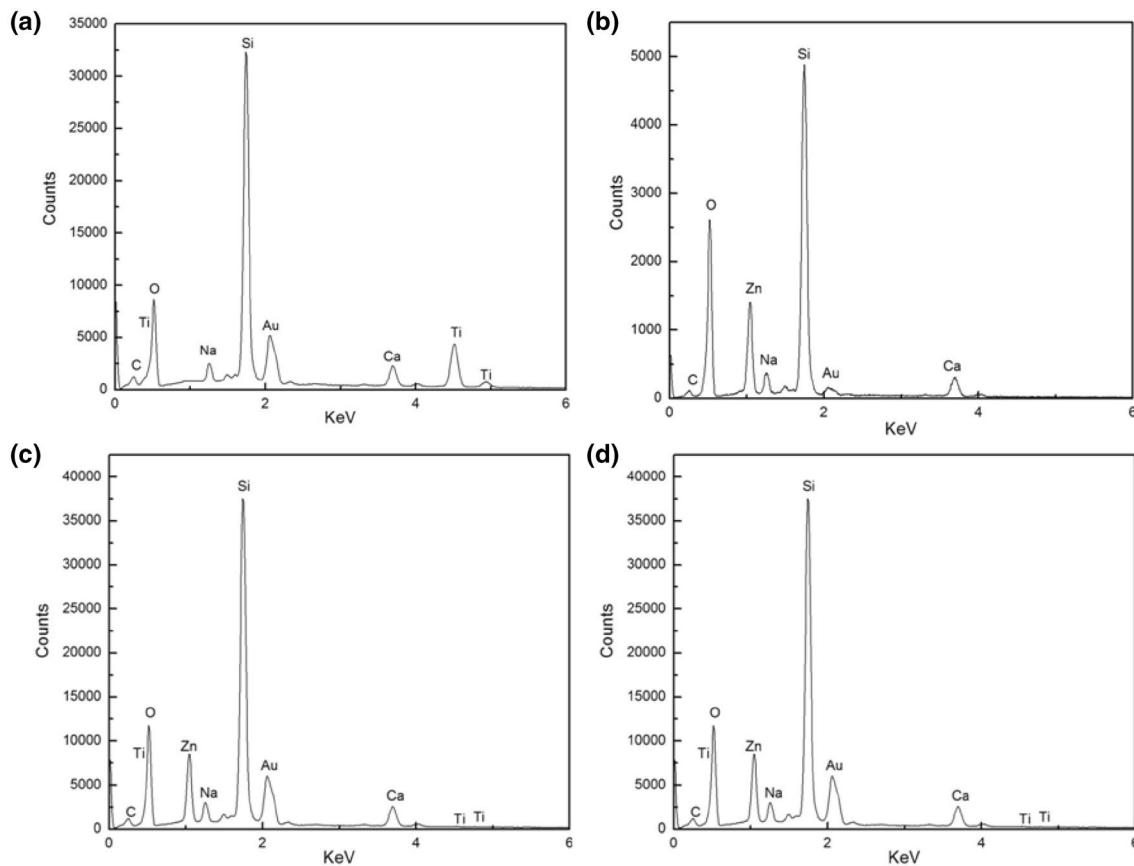**Fig. 2** FESEM micrographs of **a** TiO_2 **b** ZnO **c** TiO_2/ZnO and **d** ZnO/TiO_2 thin films
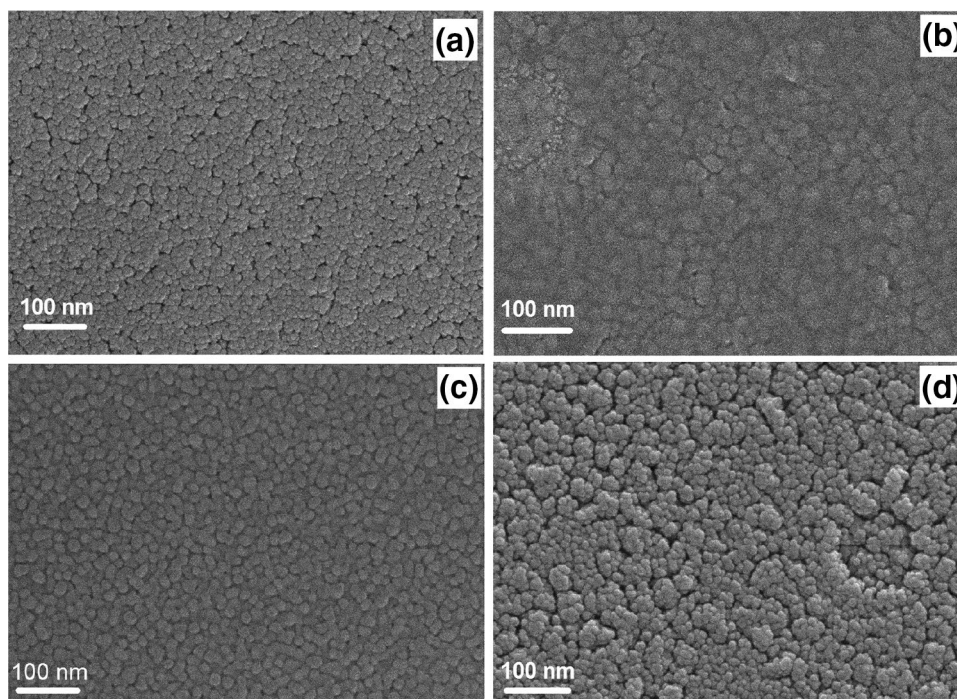
Fig. 3 EDX spectra of **a** TiO_2 **b** ZnO **c** TiO_2/ZnO and **d** ZnO/TiO_2 thin films

TiO_2 as compared to TiO_2/ZnO is responsible for its higher WCA. The hydrophilicity of the films can be attributed to the adsorption of hydroxyl group on the surface of the films deposited by sol–gel route [29]. The presence of hydroxyl groups can be confirmed by FT-IR (Fig. 4a) which shows characteristic –OH peak at 3382 cm^{-1}. The water droplet can easily spread on the surface of the film because of the interaction of water molecules with the hydroxyl group present on the surface.

Surface modification was done by immersing the samples in 8 mM octadecanoic acid dissolved in ethanol. The evidence of octadecanoic acid being grafted on ZnO/TiO_2 is confirmed by FT-IR (Fig. 4b). The peaks at 2846 cm^{-1} and 2917 cm^{-1} confirms the presence of long chain alkyl group of octadecanoic acid on the surface. The peaks at 1471 cm^{-1} and 1532 cm^{-1} are due to symmetric and asymmetric stretches of the carboxyl group. The peak at 1386 cm^{-1} is due to symmetrical stretching of carboxylate group present in octadecanoic acid [30]. The octadecanoic acid modified WCA and total surface energy of TiO_2 was 104.9º and 33.4 mJ/m^2 ($\sigma_S^D = 33.4$ mJ/m^2, $\sigma_S^P = 0$ mJ/m^2) where as the octadecanoic acid modified ZnO films has WCA and total surface energy as 125.3º and 22.0 mJ/

m^2 ($\sigma_S^D = 22.0$ mJ/m^2, $\sigma_S^P = 0$ mJ/m^2). The TiO_2/ZnO films upon modification have WCA and total surface energy as 121.3º and 26.2 mJ/m^2 ($\sigma_S^D = 26.2$ mJ/m^2, $\sigma_S^P = 0$ mJ/m^2) whereas ZnO/TiO_2 bilayer films have WCA and total surface energy as 151.0º and 18.6 mJ/m^2 ($\sigma_S^D = 18.6$ mJ/m^2, $\sigma_S^P = 0$ mJ/m^2). The superhydrophobicity of ZnO/TiO_2 is attributed to the combined effect of its large surface roughness because of the non-uniform agglomeration of particles (Fig. 2) and thin layer of low surface energy compound (octadecanoic acid). Chemical modification of the films with octadecanoic acid led to the reaction of the carboxyl group with surface hydroxyl group to form self assembled monolayer of metal-stearate bond with hydrophobic alkyl group orienting perpendicularly to the surface. It is worth noting that films modified with octadecanoic acid with suitable roughness decreases the surface energy which tunes the hydrophilic films into hydrophobic or superhydrophobic [31, 32].

The photo-induced degradation of octadecanoic acid by TiO_2, ZnO, TiO_2/ZnO and ZnO/TiO_2 was assessed by measuring the WCA after every 10 min exposure to UV light. The decrease in WCA after exposure to UV-light

Table 1 The drop profile, water contact angle (WCA) and surface energy of as deposited and octadecanoic acid modified TiO_2, ZnO, TiO_2/ZnO and ZnO/TiO_2 thin films respectively

Sample	Drop profile (water)	Contact angle (water) (°)	Surface Energy (mJ/m^2)		
			Polar	Dispersive	Total
TiO_2		16.9	41.5	29.2	70.7
ZnO		75.3	9.5	25.7	35.2
TiO_2/ZnO		26.3	36.4	30.8	67.2
ZnO/TiO_2		43.6	27.5	29.3	56.8
TiO_2 modified with octadecanoic acid		104.9	0	33.4	33.4
ZnO modified with octadecanoic acid		125.3	0	22.0	22.0
TiO_2/ZnO modified with octadecanoic acid		121.3	0	26.2	26.2
ZnO/TiO_2 modified with octadecanoic acid		151.0	0	18.6	18.6

Fig. 4 FT-IR spectra of **a** ZnO/TiO_2 and **b** ZnO/TiO_2 modified with octadecanoic acid
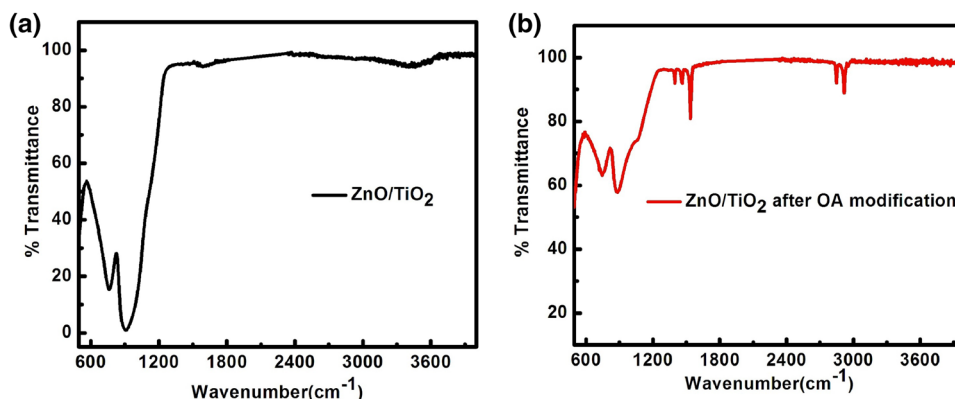
is shown in Fig. 5. It is evident that ZnO/TiO_2 becomes superhydrophilic after 50 min of UV-light exposure with WCA 2.3°. To further understand the photodegradation of octadecanoic acid under UV light, the hydrophilic conversion rate constant was calculated from the slope of reciprocal of contact angle against irradiation time (Fig. 6). The hydrophilic conversion rate was found to be 1.55×10^{-3}/degree/min, 0.35×10^{-3}/degree/min, 4.28×10^{-3}/degree/min and 6.19×10^{-3}/degree/min for TiO_2, ZnO, TiO_2/ZnO and ZnO/TiO_2 respectively.

The photodegradation of methylene blue (MB) in UV irradiation was carried out to investigate the photocatalytic performances of ZnO, TiO_2, TiO_2/ZnO and ZnO/TiO_2 films. The MB solution was made by dissolving 0.24 g of MB in 40 ml of deionized water and was stirred for 30 min. The photocatalytic films were dipped in the solution of MB
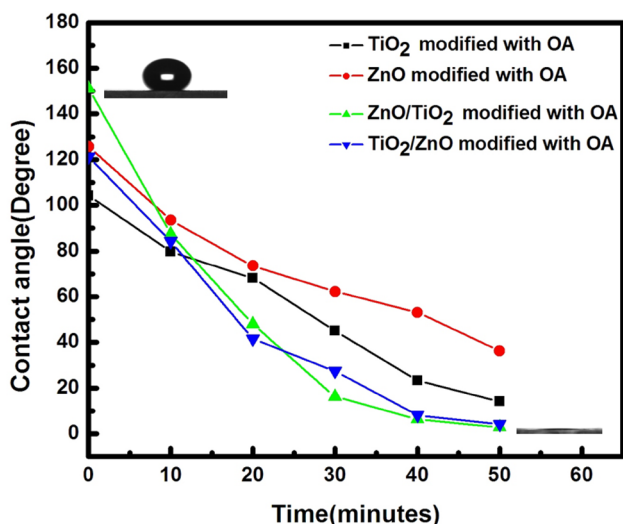
Fig. 5 Variation of water contact angle under UV Irradiation
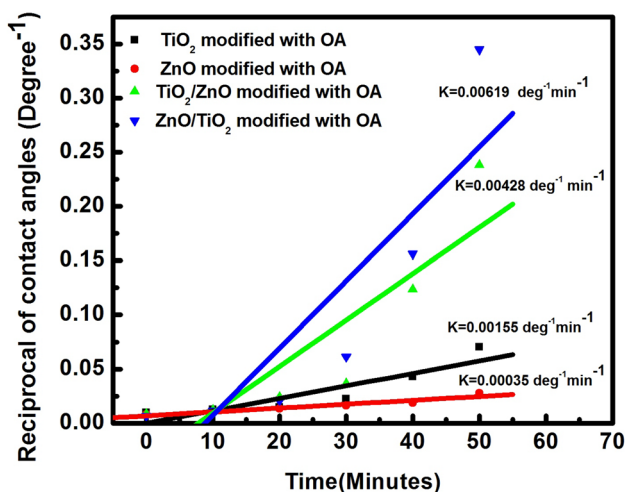

Fig. 6 Variation of reciprocal of water contact angle under UV irradiation

kept in 15 ml quartz vessel. To establish the equilibrium of adsorption–desorption process, the solution was kept in dark environment. Further the quartz vessel was illuminated with UV-C lamp (6 W, 254 nm). In order to evaluate the photocatalytic activity of the films, the absorbance of the aqueous MB solution was measured after every 30 min for 4 h. Fig. 7 shows the absorbance spectra of the aqueous MB solution upon various UV irradiation time of TiO_2, ZnO, TiO_2/ZnO and ZnO/TiO_2 thin films.

The percentage photocatalytic efficiencies of the films were evaluated using the equation.

$$\eta = \left(\frac{C_o - C}{C_o} \right) \times 100 \tag{3}$$

where C_o is the initial concentration of the MB solution and C is the concentration after irradiation time (t).

The photodegradation was calculated from the maximum absorption wavelength ($\lambda = 664$ nm). Figure 8a shows the percentage photocatalytic efficiency with UV irradiation time. From Fig. 8b, it is evident that ZnO/TiO_2 has better photocatalytic activities in comparison with TiO_2/ZnO, TiO_2 and ZnO.

To evaluate the rate of photodegradation, rate constant was determined by using pseudo first order equation.

$$\ln \left(\frac{C_o}{C} \right) = -Kt \tag{4}$$

where K is the apparent rate constant.

Figure 9 depicts the first-order reaction kinetics of TiO_2, ZnO, TiO_2/ZnO and ZnO/TiO_2 thin films. The slope of the plot $\ln(C_o/C)$ against UV irradiation time gives the rate constant. The % photocatalytic efficiencies and rate constants calculated using Eq. (3) and (4) is shown in Table 2. The % photocatalytic efficiency of TiO_2 films were found to be 82% with rate constant 0.7×10^{-2}/min where as ZnO films degrade 71% of initial MB concentration with rate constant 0.5×10^{-2}/min. There is an increase in the % photocatalytic efficiency of TiO_2/ZnO and ZnO/TiO_2 films. The efficiency of TiO_2/ZnO films was found to be 87% with rate constant 0.8×10^{-2}/min where as the efficiency of ZnO/TiO_2 films was found to be highest among the others which degrade 94% of the initial MB concentration with rate constant 1.2×10^{-2}/min.

To evaluate the adsorption capacity (in absence of light) of the photocatalyst and the durability of the dye during photolysis (only dye in presence of light), controlled experiments were carried out. The degradation of the dye carried out by these processes was found out to be negligible as compared to that by the photocatalyst. This manifests the main contribution in the photo degradation was due to the photocatalyst.

Since the change of colour alone cannot determine the mineralization of MB dye, total organic carbon (TOC) analysis was executed to understand the degree of its mineralization during the degradation process. Moreover the removal of colour during photocatalytic degradation process could give rise to more toxic intermediates than the dye itself. The analysis was done by exposing the dye in presence of photocatalyst using the same UV source. The percentage mineralization of the catalysts were evaluated using the equation.

$$\%Mineralization = \frac{(TOC)_i - (TOC)_f}{(TOC)_i} \tag{5}$$

where $(TOC)_i$ and $(TOC)_f$ is the total organic carbon before and after UV irradiation.

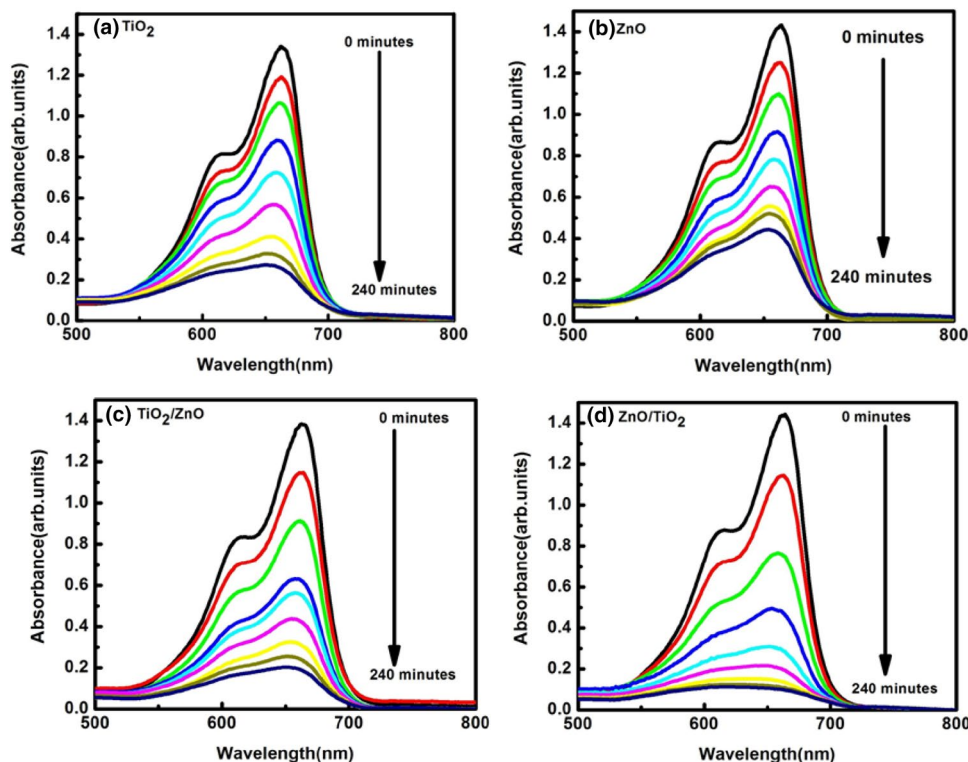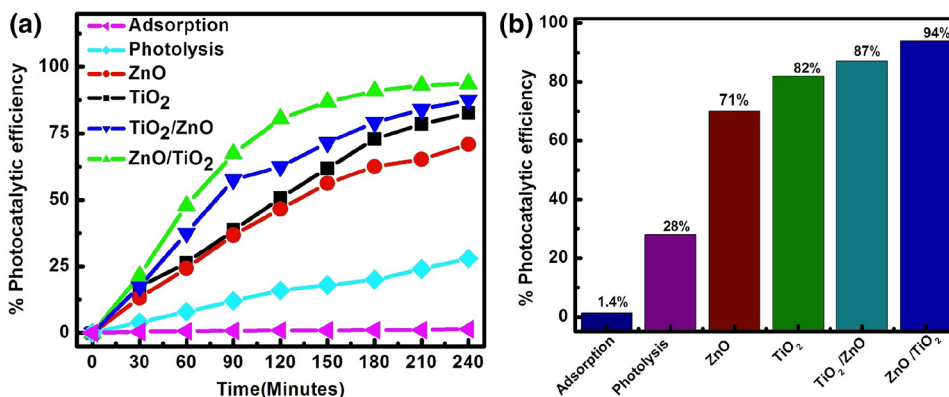**Fig. 7** UV-Visible absorbance spectra for photodegratation of MB for **a** TiO$_2$ **b** ZnO **c** TiO$_2$/ZnO **d** ZnO/TiO$_2$ thin films
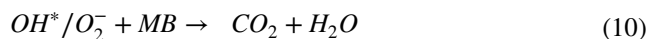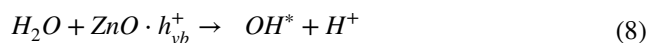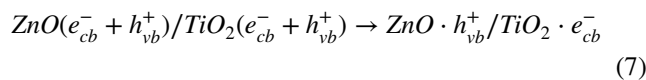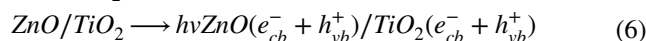

Fig. 8 a and **b** represents the % photocatalytic efficiency in the degradation of methylene blue (MB) after UV light irradiation

The mineralization efficiency of ZnO and TiO$_2$ was 37% and 42% whereas the values for TiO$_2$/ZnO and ZnO/TiO$_2$ were 46% and 49% respectively. The results indicate that the mineralization efficiency of ZnO/TiO$_2$ is highest as compared to other photocatalyst. The enhanced photocatalytic activity of ZnO/TiO$_2$ in the photo degradation of organic pollutants observed in this work is similar to the earlier reported results [33–35].

The enhanced photocatalytic and mineralization efficiency of ZnO/TiO$_2$ is accredited to the synergistic effect of TiO$_2$ and ZnO by forming a heterostructure. This facilitates the effective charge separation of electrons and holes. The

reaction mechanism for the photocatalytic activity of the ZnO/TiO$_2$ is shown below.

$$ZnO/TiO_2 \longrightarrow hvZnO(e_{cb}^- + h_{vb}^+)/TiO_2(e_{cb}^- + h_{vb}^+) \qquad (6)$$

$$ZnO(e_{cb}^- + h_{vb}^+)/TiO_2(e_{cb}^- + h_{vb}^+) \rightarrow ZnO \cdot h_{vb}^+/TiO_2 \cdot e_{cb}^- \qquad (7)$$

$$H_2O + ZnO \cdot h_{vb}^+ \rightarrow \ OH^* + H^+ \qquad (8)$$

$$O_2(ad) + TiO_2 \cdot e_{cb}^- \rightarrow \ O_2^- \qquad (9)$$

$$OH^*/O_2^- + MB \rightarrow \ CO_2 + H_2O \qquad (10)$$

The plausible photocatalytic mechanisms for charge transfer and degradation of MB using ZnO/TiO$_2$ films have
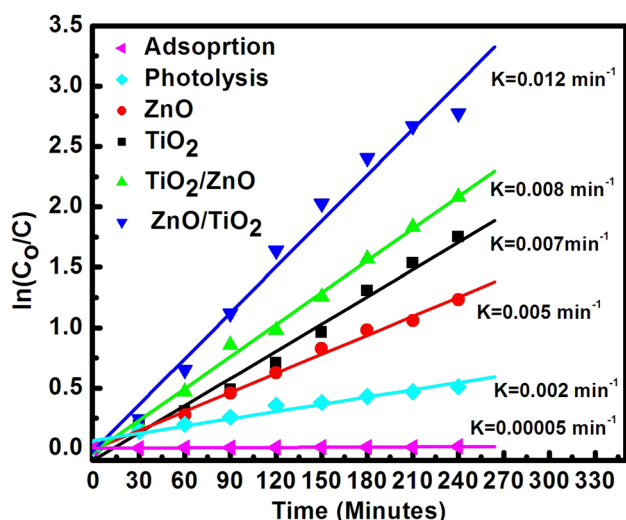
Fig. 9 Kinetics of photodegradation of MB catalyzed by TiO_2, ZnO, TiO_2/ZnO and ZnO/TiO_2 thin films under UV light irradiation

Table 2 % photocatalytic efficiency and rate constant of TiO_2, ZnO, TiO_2/ZnO and ZnO/TiO_2 thin films respectively

Samples	% photocatalytic efficiency (%)	Rate constant (min^{-1})
TiO_2	82	0.7×10^{-2}
ZnO	71	0.5×10^{-2}
TiO_2/ZnO	87	0.8×10^{-2}
ZnO/TiO_2	94	1.2×10^{-2}

been proposed. The band edge positions of conduction band (CB) and valence band (VB) of semiconductor can be determined using the following equations.

$$E_{CB} = \chi - E_e - 0.5E_g \tag{11}$$

$$E_{VB} = \chi - E_e + 0.5E_g \tag{12}$$

where χ is the absolute electronegativity of the semiconductor (χ is 5.79 eV for ZnO and 5.81 eV for TiO_2 respectively). E_g is the semiconductor band gap and E_e is the energy of free electrons on the hydrogen scale (4.5 eV). The energy band gap (E_g) of TiO_2 and ZnO is 3.26 eV. The E_{CB} and E_{VB} values for TiO_2 and ZnO calculated by using Eq. (11) and Eq. (12) are -0.32 eV and -0.34 eV and 2.94 eV and 2.92 eV respectively. The schematic representation of photocatalytic activity of ZnO/TiO_2 heterostructure is depicted in Fig. 10. In case of ZnO/TiO_2 heterostructure, ZnO is more sensitive to UV light because CB edge of ZnO is more negative than that of TiO_2 [36]. Hence upon UV irradiation electron-hole pairs from ZnO are first produced. The photogenerated electrons transfer from CB of ZnO into the CB of TiO_2. Further the photogenerated holes transferred from VB of TiO_2 to
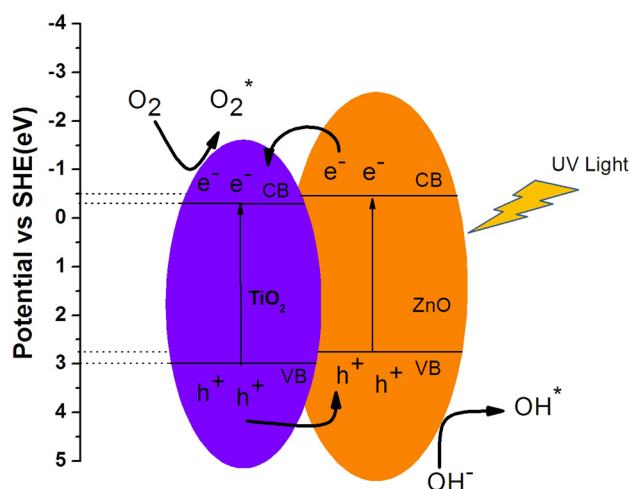

Fig. 10 Schematic illustration of reaction mechanism involved in photocatalytic activity of ZnO/TiO_2 heterostructure

the VB of ZnO due to the existence of the energy gradient at the interface between TiO_2 and ZnO [21]. Thus the interfacial charge transfer between TiO_2 and ZnO inhibits the electron–hole pair recombination. This process results in effective charge separation and increases the longevity of the charge carriers. Further the electrons in the CB of the TiO_2 react with dissolved molecular oxygen to form superoxide radicals (O_2^-) and the holes in the VB of ZnO react with surface bound H_2O to produce hydroxyl radicals (OH^*). These radicals degrade MB because of their strong reducing and oxidizing ability. Hence ZnO/TiO_2 heterostructures promotes interfacial charge transfer kinetics between ZnO and TiO_2 and improve the separation of photogenerated electron–hole pairs thereby boosting the photocatalytic activity.

4 Conclusion

Herein TiO_2, ZnO, ZnO/TiO_2 and TiO_2/ZnO thin films were synthesized by sol–gel process and deposited via spin coating method. The photocatalytic activity of ZnO/TiO_2 and TiO_2/ZnO has been studied by photodegradation of MB and octadecanoic acid under UV light. It is observed that the efficiency of biphase ZnO/TiO_2 and TiO_2/ZnO are higher than single phase ZnO and TiO_2. The rise in efficiency is attributed to the formation of heterostructure between ZnO and TiO_2 which inhibits the charge recombination. The superhydrophobicity is achieved in case of ZnO/TiO_2 thin film because of combination of low surface energy and increased roughness. The results show that ZnO/TiO_2 heterostructure acts as a universal catalyst in degradation of organic pollutants in liquid and solid phase.

References

1. C. Ray, T. Pal, J. Mater. Chem. A **5**, 9465 (2017)
2. G. Liu, L. Wang, H.G. Yang, H.M. Cheng, G.Q. Lu, J. Mater. Chem. **20**, 831 (2010)
3. N.V. Kaneva, D.T. Dimitrov, C.D. Dushkin, Appl. Surf. Sci. **257**, 8113 (2011)
4. Y. Zhiyong, Q. Ruiying, L. Huanrong, W. Zhiyin, M. Xiaohong, D. Chaonan, Mater. Lett. **170**, 25 (2016)
5. D.D. Purkayastha, R. Pandeeswari, V. Madhurima, M.G. Krishna, Mater. Lett. **92**, 151 (2013)
6. L. Znaidi, Mater. Sci. Eng., B **174**, 18 (2010)
7. Talinungsang, D.D. Purkayastha, M.G. Krishna, Appl. Surf. Sci. **447**, 724 (2018)
8. C.C. Pei, W.W.F. Leung, Catal. Commun. **37**, 100 (2013)
9. S. Banerjee, D.D. Dionysiou, S.C. Pillai, Appl. Catal. B **176**, 396 (2015)
10. R. Zhao, L. Zhu, F. Cai, Z. Yang, X. Gu, J. Huang, L. Cao, Appl. Phys. A **113**, 67 (2013)
11. W. Dong, F. Pan, L. Xu, M. Zheng, C.H. Sow, K. Wu, G.Q. Xu, W. Chen, Appl. Surf. Sci. **349**, 279 (2015)
12. B. Pal, M. Sharon, G. Nogami, Mater. Chem. Phys. **59**, 254 (1999)
13. Z. Zhang, C. Shao, X. Li, L. Zhang, H. Xue, C. Wang, Y. Liu, J. Phys. Chem. C **114**, 7920 (2010)
14. H. Cheng, C.Y. Lin, C.M. Hsu, Appl. Surf. Sci. **396**, 393 (2017)
15. M.G. Krishna, V. Madhurima, D.D. Purkayastha, Eur. Phys. J. Appl. Phys. **62**, 30001 (2013)
16. U.P. Shaik, S. Kshirsagar, M.G. Krishna, S.P. Tewari, D.D. Purkayastha, V. Madhurima, Mater. Lett. **75**, 51 (2012)
17. M. Duta, D. Perniu, A. Duta, Appl. Surf. Sci. **306**, 80 (2014)
18. W. Gao, Z. Li, Ceram. Int. **30**, 1155 (2004)
19. C. J. Brinker, G. W. Scherer, Academic press (1990)
20. D.L. Liao, C.A. Badour, B.Q. Liao, J. Photochem. Photobiol., A **194**, 11 (2008)
21. C. Sun, Q. Xu, Y. Xie, Y. Ling, Y. Hou, J. Mater. Chem. A **6**, 8289 (2018)
22. F.X. Xiao, A.C.S. Appl, Mater. Interfaces **4**, 7055 (2012)
23. P.G. Ramos, E. Flores, L.A. Sanchez, R.J. Candal, M. Hojamberdiev, W. Estrada, J. Rodriguez, Appl. Surf. Sci. **426**, 844–851 (2017)
24. M. Hemissi, H.A. Adnani, Digest J Nanomater biostruct. **2**, 299 (2007)
25. N. Kanevaa, I. Stambolovab, V. Blaskovb, Y. Dimitrievc, S. Vassilevd, C. Dushkin, J. Alloys Compd. **500**, 252 (2010)
26. F. Rahmani, M. Ardyanian, J. Mater. Sci. **29**, 4285–4293 (2018)
27. T. Young, Phil. Trans R. Soc. **95**, 65 (1805)
28. D.K. Owens, R.C. Wendt, J. Appl. Polym. Sci. **13**, 1741 (1969)
29. A.B. Gurav, S.S. Latthe, R.S. Vhatkar, J.G. Lee, D.Y. Kim, J.J. Park, S.S. Yoon, Ceram. Int. **40**, 7151 (2014)
30. J. Zhu, B. Liu, L. Li, Z. Zeng, W. Zhao, G. Wang, X. Guan, J. Phys. Chem. A **120**, 5617–5623 (2016)
31. X. Wu, L. Zheng, D. Wu, Langmuir **21**, 2665 (2005)
32. T. Rezayi, M.H. Entezari, New J. Chem. **40**, 2582 (2016)
33. R. Qin, F. Meng, M.W. Khan, B. Yu, H. Li, Z. Fan, J. Gong, Mater. Lett. **240**, 84 (2019)
34. K.S. Stefańska, A. Kubiak, A. Piasecki, A. Dobrowolska, K. Czaczyk, M. Motylenko, D. Rafaja, H. Ehrlich, T. Jesionowski, Appl. Surf. Sci. **469**, 791 (2019)
35. N.G. Menon, S.S.V. Tatiparti, S. Mukherji, Colloid Surface A **565**, 47 (2019)
36. Y. Lei, G. Zhao, M. Liu, Z. Zhang, X. Tong, T. Cao, J. Phys. Chem. C **113**, 19067 (2009)

Publisher's Note Springer Nature remains neutral with regard to jurisdictional claims in published maps and institutional affiliations.